APPLIED COMPUTING, MATHEMATICS AND STATISTICS GROUP
Division of Applied Management and Computing

Study of fracture properties of wood using high-speed video Imaging and neural networks

Sandhya Samarasinghe and Don Kulasiri

Research Report 03/2002
April 2002

ISSN 1174-6696

RESEARCH REPORT

LINCOLN UNIVERSITY
Te Whare Wānaka O Aoraki

Applied Computing, Mathematics and Statistics

The Applied Computing, Mathematics and Statistics Group (ACMS) comprises staff of the Applied Management and Computing Division at Lincoln University whose research and teaching interests are in computing and quantitative disciplines. Previously this group was the academic section of the Centre for Computing and Biometrics at Lincoln University.

The group teaches subjects leading to a Bachelor of Applied Computing degree and a computing major in the Bachelor of Commerce and Management. In addition, it contributes computing, statistics and mathematics subjects to a wide range of other Lincoln University degrees. In particular students can take a computing and mathematics major in the BSc.

The ACMS group is strongly involved in postgraduate teaching leading to honours, masters and PhD degrees. Research interests are in modelling and simulation, applied statistics, end user computing, computer assisted learning, aspects of computer networking, geometric modelling and visualisation.

Research Reports

Every paper appearing in this series has undergone editorial review within the ACMS group. The editorial panel is selected by an editor who is appointed by the Chair of the Applied Management and Computing Division Research Committee.

The views expressed in this paper are not necessarily the same as those held by members of the editorial panel. The accuracy of the information presented in this paper is the sole responsibility of the authors.

This series is a continuation of the series "Centre for Computing and Biometrics Research Report" ISSN 1173-8405.

Copyright

Correspondence

This paper represents work to date and may not necessarily form the basis for the authors' final conclusions relating to this topic. It is likely, however, that the paper will appear in some form in a journal or in conference proceedings in the near future. The authors would be pleased to receive correspondence in connection with any of the issues raised in this paper. Please contact the authors either by email or by writing to the address below.

Any correspondence concerning the series should be sent to:

The Editor
Applied Computing, Mathematics and Statistics Group
Applied Management and Computing Division
PO Box 84
Lincoln University
Canterbury
NEW ZEALAND

Email: computing@lincoln.ac.nz

Study of fracture properties of wood using high-speed video imaging and neural networks

Sandhya Samarasinghe
Centre for Advanced Computational Solutions (C-fACS) &
Natural Resources Engineering Group
and

Don Kualsiri
Centre for Advanced Computational Solutions (C-fACS) &
Applied Computing, Mathematics and Statistics Group
Lincoln University
Canterbury, New Zealand

Abstract

In this study, the Duration of Load (DOL) for crack initiation and propagation, crack speed, and load carrying capacity were investigated for three Rates of Loading (ROL) and four sizes of notched wood beams using high-speed video imaging and neural networks. For the smallest ROL, there was a distinct volume effect on DOL to initiation which was almost inhibited at the largest ROL. The DOL for crack propagation for all volumes appeared to be random. The crack propagation was a wave phenomenon with positive and negative speeds that varied with the rate of loading. The study showed that the crack initiation load, peak load, and their respective gross stresses were independent of ROL but were nonlinealry correlated with volume and the smallest volume maintained the highest stress. The stresses followed the Weibull's weakest link theory. Artificial Neural networks (ANN) revealed meaningful trends for the combined effect of physical and geometric variables on the loads and stresses. Fracture toughness was insensitive to ROL and realtively constant for the three larger volumes. However, the smallest size produced the largest fracture toughness, which was explained by a neural network model that showed that the width had the greatest influence on fracture toughness highlighting plane stress conditions. The study showed the usefulness of ANN for analyzing interaction among many variables affecting wood fracture behaviour and their ptential to become reliable predictors of load carrying capacity including maximum load and stress and fracture toughness under the uncertain influence of these variables.

Key words: *fracture dynamics, fracture toughness, load-carrying capacity, high-speed video imaging, neural networks, duration of load, crack speed, New Zealand pinus radiata*

1. Introduction

Many materials, particularly biological and cellular materials such as wood, contain micro- or macro-voids that initiate a crack to propagate once enough stress is concentrated in the vicinity of these voids. A substantial amount of work has been done on fracture of wood and crack tip displacements (Patton-Mallory, 1987; Samarasinghe and Kulasiri, 2000(a); Samarasinghe and Kulasiri, 2000(b), Bandara et al., 1999, Samarasinghe and Kulasiri, 1999, Samarasinghe and Kulasiri, 1998)). However, very little has been done to understand fracture dynamics of wood, which includes duration of load (DOL) and speed of crack propagation. The DOL is measure of the survival time of a member under load; therefore, how the presence of a crack influences DOL is useful in the design of structures.

Neilsen (1978) defined two failure states in which (i) material damage starts or crack propagation is initiated, and (ii) the damage level has reached a point where there is no load carrying capacity left and the rate of crack propagation increases

catastrophically. The time to reach any of these failure states is said to be the time to failure or the duration of load (DOL). The first case is the lower limit of failure (safe mode, or DOL to crack initiation) and the second case is the upper limit, or DOL to catastrophic failure. We use these two definitions and focus on DOL to initiation and DOL for propagation of a crack and how they are affected by size and ROL. The latter indicates the survival time of a member once a crack has started to propagate. Crack speed indicates the rate of propagation of a crack and it increases our knowledge of the energy dissipation within the material.

It would be of much practical use, if load carrying capacity of *a particular cracked beam* can be predicted from its basic physical and geometric variables. Our understanding of the size and ROL on fracture resistance is currently limited. Fracture of wood in relation to moisture content, temperature, density, and size has been studied separately. However, little is known about the combined effect of the size, ROL, physical variables, such as moisture content, density, and Young's Modulus, as well as geometric variables, such as grain angle, ring (face) angle and curvature of growth rings on fracture resistance of a particular wood member. A common experience in wood testing is the large scatter of the data. In this study, we hypothesized that the scatter may be due to these multi-dimensional data being projected on to two dimensions and a realistic picture can be seen if all the interactions are taken into account, which has not been done in the past.

Neural networks are powerful computational methods that enable the development of complex models that capture the underlying relationship between a multitude of variables. In this study, we investigate the ability of Neural Network models to predict load carrying capacity of cracked beams from its size, rate of loading, and physical and geometric variables. If successful, the method could provide a complimentary or an alternative approach to fracture mechanics for predicting strength of cracked wood members under the uncertain influence of physical and geometric variables.

2. Objectives

This research aims to study, systematically and step-by-step, several issues related to crack propagation in wood beams with a sharp crack perpendicular to the grain. Specifically, we aim to:

- Study the Duration of Load (DOL) to initiation and DOL for propagation and their dependence on size and rate of loading (ROL),

- Determine the speed of a propagating crack using high speed imaging and its relationship to rate of loading,

- Develop of Neural Network models to predict load and stress at crack initiation and peak response from size, rate of loading, density, moisture content, Young's modulus, grain angle, ring angle, and curvature of growth rings,

- Determine the stress intensity factor at crack initiation and its dependence on the size, ROL and other physical and geometric variables.

3. Background

3.1 Duration of load for fracture

Spencer (1978) studied the duration of load of solid wood beams under various rates of loading. He found that the higher the rate of loading, the lower the duration of load. However, for any rate of loading, the 95th percentile held the load the longest and the 5th percentile held the load the shortest duration. The 5th percentile pieces in Spencer's (1978) study must be the weaker ones containing some strength reducing defects such as knots, large slope of grain etc. Therefore, it can be intuited that beams containing a crack would fail more quickly than a defect free solid beam at any rate of loading. However, how the rate of loading affects the time to failure of notched beams needs investigation.

3.2. Velocity of propagating cracks

Mindness et al. (1978) developed the following relationship between velocity of crack propagation, u, and fracture toughness, K_{Ic}, from experiments carried out on Douglas-fir:

$$\ln u = n \ln K_{Ic} + \ln A \qquad [1]$$

where, A and n are constants. This shows that the initial crack speed increases with the fracture toughness of the material.

3.3. Size and rate of loading effect on strength

Weibull in 1939 derived a mathematical formulation based on the weakest link theory to demonstrate that the strength of a material is negatively correlated with volume (Madsen, 1992). Based on this theory, Bohonen (1966, in Madsen, 1992) found that the length*depth was a better predictor of solid wood strength than the volume, and Pederson (1999) showed that the solid wood strength depended on height, not on volume or length*depth. Pederson (1999) also stated that the size effect is more significant for smaller volumes.

Bending tests carried out on notched and solid specimens under various loading conditions have shown that the strength of solid beams increases with increasing ROL; however, the strength of notched beams remain unaffected by it (Madsen, 1992). Spencer (1978) tested D. fir solid beams at eight 8 ROLs and found that the strength was insensitive to ROL up to about 50^{th} percentile strength. However, the strength of higher percentiles increased with ROL and the effect was intensified as percentile increased towards the 95^{th} percentile. Therefore, if we assume that lower percentiles contain strength reducing defects, observations of these two investigators indicate that the damaging effect of creep is eliminated in wood containing cracks.

3.4. Fracture toughness

Fracture toughness is a measure of the strength of a cracked member and is considered a material property. It is a parameter found in the linear elastic fracture mechanics formulation and it uniquely defines the stress distribution surrounding a crack at the point of failure (Sih et al., 1965). Fracture toughness is generally obtained from experiments conducted on specimens containing a crack and using formulae found in stress intensity factor handbooks. Fracture toughness is denoted by K_c and an additional subscript, I, II, or III, is added to indicate opening, shearing and out of plane fracture, respectively. Formulation of fracture theories assumes co-linear crack propagation. In wood beams however, cracks propagate perpendicular to the existing crack (i.e. parallel-to-grain). In wood literature, the associated fracture toughness is called K_{Ic} perpendicular to the grain (LT or LR mode of propagation)

where the original crack is perpendicular to grain and theoretical propagation direction is R or T.

3.4.1. Effects of rate of loading, size and physical properties on fracture toughness

Schniewind et al. (1978) found from creep studies on notched and knotty beams that fracture toughness increased with decreasing ROL thus eliminating the need for a load duration factor. They made the same observation for ramp loaded notched beams. Schniewind et al. (1978) further reports that Leicester (1974), who ramp tested notched beams to fail from 1 to 300 minutes, found the maximum fracture toughness for 30-minute duration. These observations bear resemblance to the findings of earlier mentioned investigators that the strength of notched beams is not affected by ROL.

Stanzl-Tschegg et al. (1995) found that the fracture toughness increased with ligament length and it also increased with thickness up to a point and then decreased. Barrett and Foschi (1978) found that K_{IC} for cracks propagating along the grain in Douglas-fir specimens decreased with thickness. Similar increase in fracture toughness for thinner thickness sections has been established for other materials due to plane stress conditions. Boatright and Garrett (in Patton Mallory, 1987) used the variation in stress state across the crack front and the occurrence of irreversible deformation (cell buckling) to explain the higher K_{IC} in thinner thickness.

Johnson (1973) found that the variation of $K_{Ic(TL)}$ (cracks perpendicular to T direction and propagating in L direction) was insensitive to initial crack length and thickness. Porter (1964) found that the Strain energy release rate (G_{IC}) to be independent of specimen length, thickness and height as well as crack length in both TL and RL planes. (G_{IC} is a measure of the rate of release of strain energy in fracture and is related to K_{IC} through Young's modulus).

Petterson and Bodig (1982) found that the fracture toughness ($K_{Ic(TL)}$) increased with specific gravity in the form of a power function and decreased with moisture content. Smith and Chui (1993) studied the effect of moisture content, density and the orientation (θ) of the original crack in the RT plane (measured as the angle between crack plane and tangent to growth ring) on critical strain energy release rate G_{Ic} of tensile specimens. They found that G_{IC} increased from fibre saturation

down to about 18% and then decreased with further decrease in moisture content contradicting the continuously decreasing trend down to dry conditions found by Petterson and Bodig (1983). Smith and Chui (1993) state that the relationship between G_{IC} and density becomes stronger as moisture content decreases.

Smith and Chui (1993) also found that G_{IC} increased with decreasing θ down to 60° but decreased with further decrease in angle. Although the authors did not discuss the reasons for this trend, it can be explained as follows: When the angle is 90°, the crack plane coincides with the weak RL plane and therefore, a lower G_{IC} can be expected. Similarly, when the angle is 0°, crack plane coincides with the TL plane, which is also weak due to earlywood-latewood boundaries. Therefore, a lower G_{IC} can again be intuited. Thus, the maximum G_{IC} can be expected for an intermediate orientation of the crack plane as found by these investigators.

4. Neural networks summary

The development of Artificial Neural Networks (ANN) was inspired by the information processing and learning mechanisms in biological neural networks in the brain that are massively parallel computing systems consisting of an extremely large number of simple processors with many interconnections. Neural Networks are especially suitable for approximating functions of many variables (Haykin, 1994, Smith 1996), and they are capable of mapping any nonlinear function to any desired degree of accuracy. They have been shown to be superior to statistical methods in nonlinear modelling (Smith 1996).

Following is a brief review of neural networks. Figure 1 shows the operation of a basic feed-forward Multi-Layer Perceptron (MLP) network consisting of an input layer of neurons, hidden layer of neurons and an output neuron. Each input neuron represents one input variable and the output neuron represents the output variable. Information passes forward (feed-forward) from input through hidden to output layers to generate an output as follows: An input vector containing a value for each input variable (i) is presented to the input layer which passes it to each hidden layer neuron (j) via designated weights (w_{ij}). Each hidden layer neuron (j) does two functions: (1) it calculates the weighted sum (u_j) of n inputs (x_i) that it receives, and (2) passes this sum through an activation function $g(u_j)$ to produce a hidden neuron output (y_j) as follows:

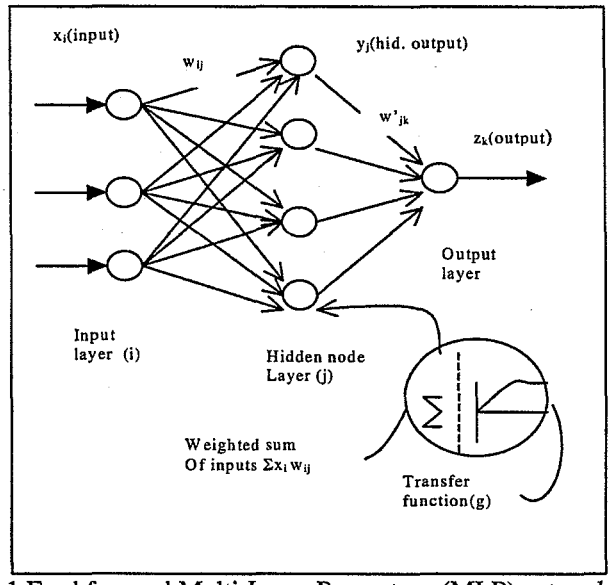

Fig. 1 Feed forward Multi-Layer Perceptron (MLP) network

$$u_j = \sum_{i=1}^{n} x_i w_{ij} \qquad [2]$$

$$y_j = g(u_j) \qquad [3]$$

Some commonly known activation functions are sigmoid (that include logistic functions), Gaussian, linear, and threshold functions. The hidden layer output y_j of m neurons is then transmitted through their weights (w'_{jk}) to the output neuron (k), which calculates the weighted sum (v_k) and passes this through its activation function $f(v_k)$ to produce the desired output (z_k) as follows:

$$v_k = \sum_{j=1}^{m} y_j w_{jk} \qquad [4]$$

$$z_k = f(v_k) \qquad [5]$$

where k is the number of output neurons and is equal to 1 for a single output.

In neural network development, a network is "trained" by exposing the same data set over and over while processing one input vector at a time until the network

"learns" the underlying relationship. At the beginning, the weights are set randomly and therefore, the desired output is far from the expected value. In the training of the network, this is corrected by a learning mechanism and a well-known method is error back propagation which is a gradient descent approach. Basically, the training in neural networks involves incremental adjustment of all the weights until prediction error reaches a minimum acceptable level as follows: After the network output is obtained for a given input vector, the difference (Error, E) between the predicted (z_k) and the expected output is calculated. Then the gradient of the error (partial derivative) with respect to each of the hidden-output layer weights (w'_{ij}) is obtained by using the chain rule of differentiation:

$$\frac{\partial E}{\partial w'_{jk}} = \frac{\partial E}{\partial z_k} \frac{\partial z_k}{\partial v_k} \frac{dv_k}{\partial w'_{jk}} \qquad [6]$$

Gradients for input-output layer weights (w_{ij}) are computed similarly. Each of these error gradients, for a given input vector, indicates the direction of the network error increase with respect to the weight it represents after processing one input vector. The whole set of input vectors (n) are processed (one epoch) in this manner and the average error gradient (d'_{jk}) for a hidden neuron weight, w'_{jk}, is calculated as follows:

$$d'_{jk} = \sum_{i=1}^{n} \left(\frac{\partial E}{\partial w'_{jk}}\right)_i \qquad [7]$$

The average error gradient indicates the direction of the *average* error increase for a particular weight. The value of the weight is adjusted after each epoch by a fraction in the direction of the negative error gradient by multiplying the error gradient by a factor (ε) called the learning rate which is a constant between 0 and 1 (Eq.(8)). This process is repeated by processing the input data set over and over through many epochs, until the optimum weights are found and the prediction error settles down to a minimum acceptable level.

$$\Delta w'_{jk\,(m)} = \varepsilon\, d'_{jk\,(m)} \qquad [8]$$

Based on this basic idea, several variants of back propagation have been developed to speed up the training process. A similar calculation is done for adjusting the input-hidden layer weights. The factors that are generally altered in search of the optimum network are: the number of neurons in the hidden layer, that gives the network the ability to map complex nonlinear functions and generalise; initial weights which expedites the search for the global minimum of the error function; activation functions that adjust themselves to follow the nonlinear trends in the data; learning rate and related parameters. The data set is divided into training, testing and validation sets and these are used for training, testing the accuracy while training, and validating the trained networks, respectively.

Seibi and Al-Alawi (1997) developed a feed-forward Multi-Layer Perceptron (MLP) Neural Network to investigate the effect of crack geometry, temperature and loading on fracture toughness of 7075-T651 aluminium alloy beams and plates containing surface and through-thickness cracks. Their model resulted in an R^2 value greater than 0.95 indicating that the network has captured a very strong relationship between the input variables and fracture toughness. They also used the developed NN model to assess the contribution of individual input variables and found that temperature had a predominant influence followed by crack length to plate length ratio and crack depth to crack length ratio. They also found that the loading configuration, whether uni-axial or biaxial, played an insignificant role. Such sensitivity analysis in ANN is very useful for filtering variables that are significant for prediction. By using the developed model for analysing trends for scenarios not used in the training and testing of the ANN, the authors demonstrated the benefit of neural networks as an analytical tool.

5. Methodology

5.1. Specimen preparation and testing procedure

The specimens were prepared from kiln-dried boards cut from a log of New Zealand pinus radiata aged 30 years and especially bought for this research. Specimen configuration is shown in Figure 2 and specimen dimensions are in Table 1. There were 4 size categories (A,B,C,D) and each category had 51 specimens that were further divided into three sets for testing at three rates of loading. Specifically, 24

Table 1. Specimen sizes, rates of loading, geometric proportions, and sample sizes

Size Category	Size (L x h x b) mm	No. of specimens for each ROL (mm/min) 2.5	10.0	0.625	Crack Length (a)(mm)	a/h	Volume Ratios	Area Ratios	Dimension Ratios
A	1000 x 90 x 45	24	15	12	41	0.46	297	44	6.7
B	600 x 54 x 27	24	15	12	25	0.46	64	16	4
C	300 x 27 x 13.5	24	15	12	13	0.48	8	4	2
D	150 x 13.5 x 6.75	24	15	12	6	0.45	1	1	1

specimens were tested at 2.5 mm/min, 15 at 10 mm/min and 12 at 0.625mm/min. There were a total of 204 specimens. Table 1 also shows the volume, area, and dimension proportions that held for all forms of volume, area, and dimensions (i.e. net, gross, areas in RL and TL planes etc.)

Cracks were made by first cutting a notch with a band saw and then sharpening it with a knife edge especially prepared for each specimen size to conform to ASTM standards for metals (1995) recommendation for crack length: $0.45H \leq a \leq 0.55H$). The maximum knife-edge cut was about 2 mm and the final crack length is shown in Table 1. Height to width was maintained at the recommended ratio of 2.0. Moisture content of specimens were not controlled and boards were kept in a laboratory where the interior environment was not controlled either. This provided a range of moisture content from 4 to 16% that reflected the EMC conditions of an unheated building.

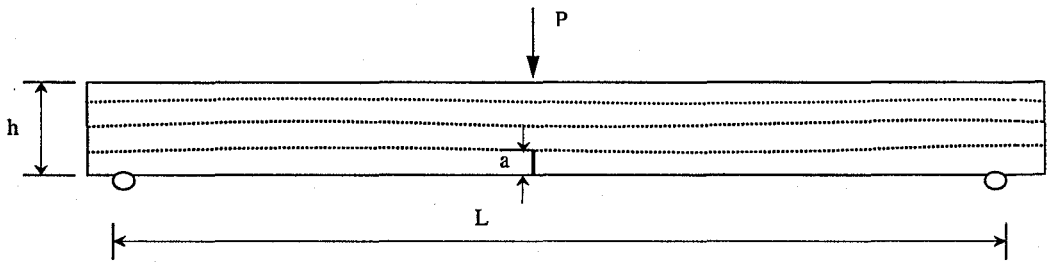

Fig. 2. Configuration of cracked beams

From the total batch of specimens, 68 had their entire crack propagation recorded on a high-speed video camera and their spread among the three loading rates for each of the four sizes was: 5 specimens for 10 mm/min, 8 for 2.5 mm/min, and 4

for 0.625 mm/min. Tests were carried out on a computer driven SINTECH (MTS) 30/D material testing workstation. Four cylindrical load applicators were made one for each size according to ASTM standards for wood (1995) and a roller bed with adjustable spans were built to accommodate specimens with different spans. The supporting experimental resources were as follows: High-speed (450 frames/sec) video camera HSC 250x2 of JC Labs Inc., high speed recording device (SVHS Panasonic AG5700 video cassette and recorder) and a monitor, two light sources to illuminate the surface of the specimens and an electronic timer with a stop watch with an accuracy of 0.01 seconds.

Figures 3 shows the experimental test set-up. The following is a description of the procedure used for high-speed video imaging of the process of crack propagation of the subset of 68 beams: The crack tip area was sprayed with black paint and the specimen was placed on the roller bed and the specimen surface was illuminated to obtain a clear image. A graph paper was placed on the specimen and its image was recorded to calibrate the image distance to real distances. The timer was hung on the specimen closer to the crack and reset and it was used to refer the images to load-time graphs obtained from the testing machine.

The load was applied at the rates specified in Table 1 and the high-speed camera was simultaneously activated. Video images of the specimen was recorded throughout the whole loading process until the specimen failed completely and 68 fracture processes were thus recorded. Load-deflection-time plots were also obtained

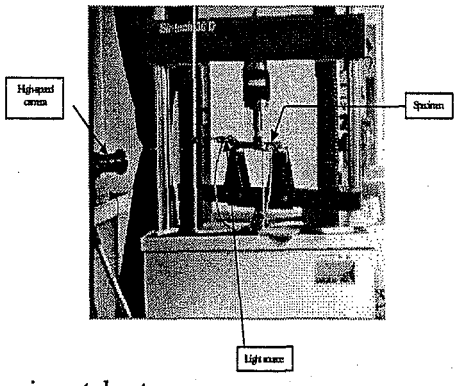

Fig. 3. Experimental setup

from the calibrated testing machine to determine loads for crack initiation and catastrophic failure, and duration of load for these events. The rest of the 136 beams were tested to failure in a similar fashion except that the crack propagation was not video recorded. For these, only the load-deflection plots were obtained. Total data set, however, was used for the study of load carrying capacity.

5.2. Measurement of physical and geometric variables

Data obtained for each specimens were: crack length, dimensions, density, moisture content, Young's modulus, ring angle, grain angle and curvature of growth rings. Soon after testing, two pieces near the tip were cut from every specimen to determine moisture content and density using the oven dry method. Young's modulus for each cracked beam was estimated from its load-deflection plot and net section of the beam. Although these values seemed to underestimate probable actual values, they were thought to be representative of the stiffness of a particular beam because the values were obtained from the same fracture specimen rather than from a separate one. Additionally, the grain angle (angle between grain and longitudinal axis of beam), face or ring angle (angle between width and tangent to a growth ring on the cross section), and ring curvature were measured as parameters defining the subsequent crack path. The range of the values for each variable was: moisture content (4-16%), grain angle (0.06° to 29°), face angle (0° to 80°), curvature (0.001 to 49.6), density (355 to 645 kg/m^3), and Young's Modulus (MOE) (1.36 to 6.11 GPa).

6. Results and Discussion

6.1 Some experimental observations

The recorded videos were played back to observe the process of crack initiation and propagation. Following is a summary of some interesting observations made from these tapes. Propagation in more than 40% of specimens did not start right from the existing crack tip. This means that stress in the whole tip region, not necessarily the crack tip stress, governs the crack initiation for these specimens. All those cracks not originating from the tip subsequently joined the tip. In most of the specimens, cracks propagated along the grain. In few cases, a multitude of small cracks developed in

different layers in the vicinity of the crack and fracture occurred in a staggered condition along some of these small cracks.

Another interesting feature observed was the crack extension and closure at high speeds indicating that fracture is not solely a forward propagating process. The crack closure indicates that crack lips close at the tip reducing the crack length. We observed a wave pattern for crack propagation with oscillations that increased rapidly as the catastrophic failure was reached. A similar wave phenomenon was reported by Abraham (1997) for isotropic materials.

6.2 DOL for crack initiation and propagation

Figure 4 shows a typical load-time plot for the beams. At the beginning, load increased uniformly with extension; however, at crack initiation graph bends and becomes nonlinear (point M in Figure 4). This time was recorded as the time to crack initiation and the corresponding load was recorded. Beyond crack initiation load increases further up to the peak load at which point the load drops suddenly to pick up again and fail catastrophically at a later time (point F in Figure 4). This was the most common form of load-time relationship. The variations were one in which load increased linearly up to the peak load and another in which peak load coincided with the catastrophic load. From each plot, the time to catastrophic failure and the corresponding load were also obtained. The peak load was also taken from the graph as the highest load reached.

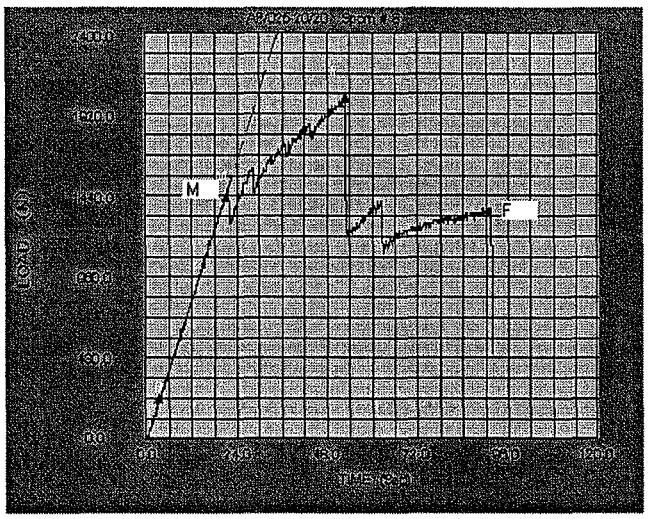

Fig. 4. A typical load-time graph indicating crack initiation (M) and catastrophic failure (F) events

6.2.1. Influence of size and ROL on DOL to crack initiation

DOL to initiation was very consistent for each volume and ROL. Figure 5 shows the influence of ROL and volume on time to crack initiation.

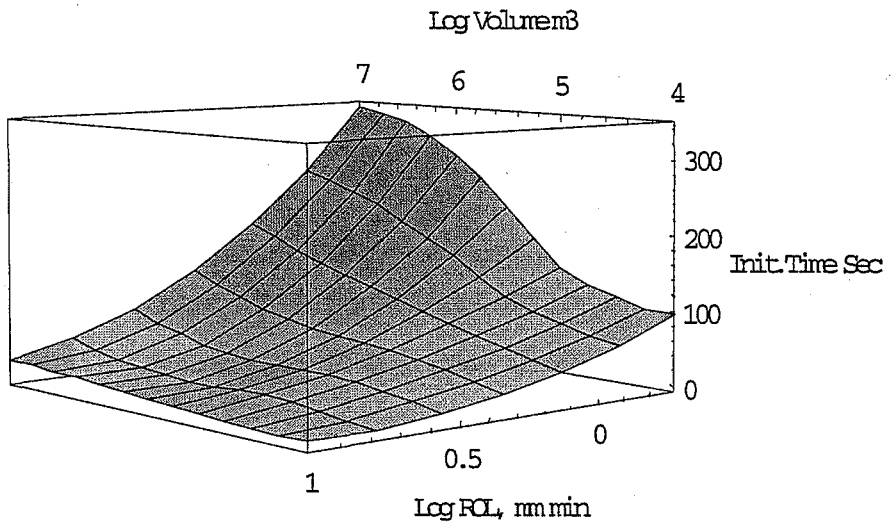

Fig. 5. Effect of volume and rate of loading on Duration of load to crack initiation

The figure shows that larger the volume longer the time, and lower the ROL longer the time to crack initiation. However, this interaction is not nonlinear. For example, there is a pronounced effect of volume at the lowest ROL (0.625 mm/min). However, this effect diminishes as ROL increases and at the highest ROL (10 mm/min), the volume effect is almost negligible. Similarly, there is a more pronounced negative influence of ROL on the largest volume than on the smaller ones. The results indicate that, under creep conditions, larger volumes could hold the load disproportionately longer than smaller volumes.

6.2.2. Influence of size and ROL on duration of crack propagation

The most significant observation regarding the duration of crack propagation was that it appeared to be highly random. This was in contrast to the time to crack initiation that was very consistent. Therefore, an average value for the duration of fracture was of little meaning and the whole range of observations are plotted in Figure 6 against volume and ROL.

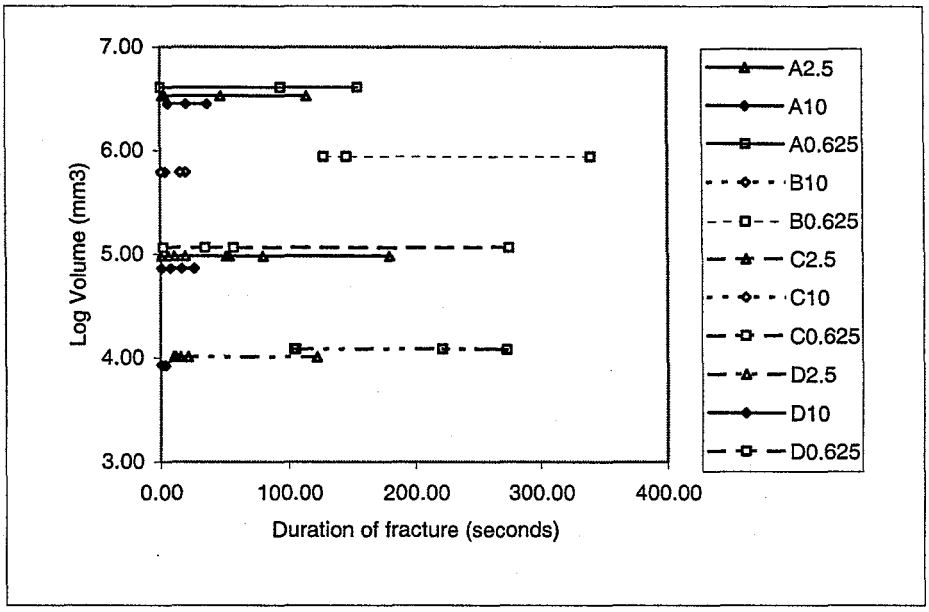

Fig. 6. Volume and ROL effect on duration of fracture for the four sizes (A,B,C,D) and 3 rates of loading

The Figure shows that once the crack propagation has initiated, a beam can fail at any time regardless of the volume. However, Figure 6 also points to the possibility that, for very low rates of loading, larger volumes may have a higher probability of failing sooner than smaller volumes, indicating that failure is more imminent for larger volumes once a crack has started to propagate. Due to the small sample size, probability distributions were not investigated; however, this phenomenon requires further investigation.

6.3. Measurement of variation of crack length and crack speed

The fracture process for all the specimens were recorded on 3-hour SVHS videotapes resulting in 9 hours worth of information. One of the drawbacks in the use of the digitized video images was the hard disk space required to store them. For example, 2-3 minute duration of video occupied about 100 MB space. Therefore, important still images, between 20 – 100 images along with the graph scale image per specimen, were captured from the tapes at appropriate events using Vedium Movie Clip multimedia imaging software and relevant hardware (1998.). Graph scale was used to convert image pixel distances to mm. For a digital image, the smallest unit is called a pixel, or picture element and the image size in this study was 512x512 pixels.

The crack length over time was computed using the crack tip coordinates obtained at the beginning and end of a specified time period. If there was a

reasonable bend in the crack during a time period, it was considered as two cracks joined at the bend and this required the calculation of the net crack length for a given time period. The net crack speed during the same time period was calculated by dividing the net crack length by the time interval. A module in C++ programming environment was created to manipulate the data arranged in Dbase IV for calculating the net crack length and speed for various time intervals throughout the fracture process.

6.3.1 Crack speed profiles

Figures 7 (a) and (b) show crack speed profiles within the time duration of fracture for two typical specimens of the largest size A (1000x90x45) for the minimum and maximum rates of loading tested. Figure 7(a) shows that the crack speed is very low at the lowest rate (0.625 mm/min) up to the catastrophic failure state where crack speed jumps rapidly in the form of a spike up to about 120 mm/sec. This indicates slow and stable crack propagation until catastrophic failure.

At the highest rate of loading (10 mm/min) however, speed fluctuates significantly throughout the fracture process with many oscillations with an overall increase up to the catastrophic failure where speed reaches about 100 mm/sec (Figure 7(b)). This profile indicates a fast and turbulent mode of crack extension at the highest ROL. At the intermediate rate of 2.5 mm/min, an intermediate scenario between those found for the smallest and highest rate of loading was observed. Here, oscillations appeared towards the end of the fracture process although they were not as frequent as for the highest rate.

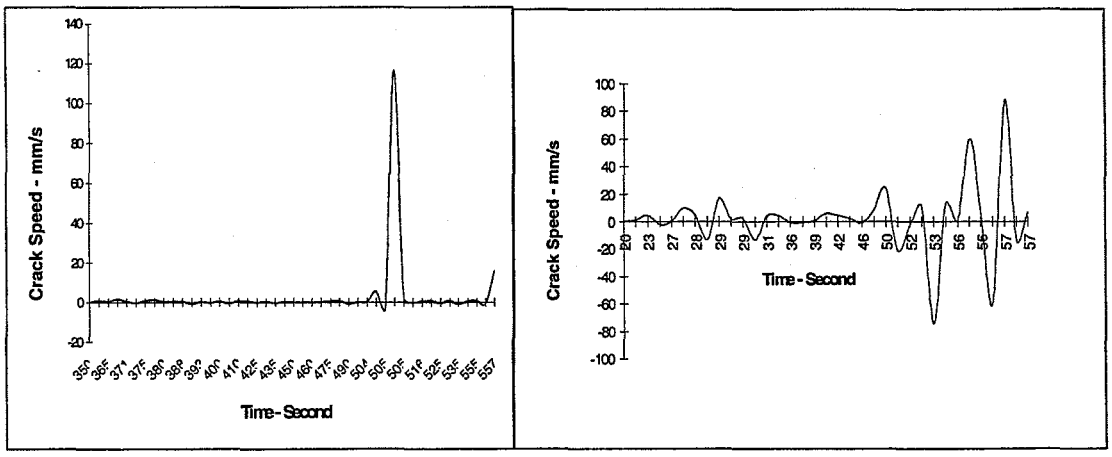

(a) (b)

Fig. 7 Crack speed profiles for a typical 1040x90x45 specimen for the rates of: (a) 0.625mm/min, (b) 10 mm/min

The negative speed indicates crack closure where crack lips touch each other thereby reducing the net crack length. This crack closure was predominant in the vicinity of the catastrophic failure. Neilsen (1978) used an assumption of non-negative crack speeds in the time interval between crack initiation and catastrophic failure to derive expressions for the time to catastrophic failure. According to our study however, alternate negative and positive speeds were quite frequent and negative speeds are reasonably high in many cases and quite significant for the higher rates of loading. The speed profiles for the other two sizes are not ready due to the labour and time intensive extraction of data from the digitized images. Therefore, the size effect on crack speed and the originally intended computer simulation of crack propagation are not studied at this point.

6.4 Peak Load and crack initiation load

6.4.1 Peak Load

A notable observation was that the peak load for all 204 specimens was very consistent. A similar observation was made by Boontanjay (1979) for notched pinus radiata beams. Figure 8(a) shows a plot of average peak load against log volume for the three rates of loading and Figure 8(b) shows a plot of raw peak load data against volume for all speeds. Figure 8(a) shows that the average load varies in the form of a power function. It also reveals that the effect of volume is very pronounced where as that of ROL is not. This is one of the most significant observations of this study and it supports the previous limited observations that the ROL either does not influence fracture strength of wood (Masden, 1992) or very low ROL might increase it (Schniewind (1978). For solid wood, it has been established that ROL affects load carrying capacity due to viscoelastic effects.

The insignificant influence of ROL poses new questions about the viscoelastic effects on wood containing a crack. It appears that the strain energy in cracked specimens is dissipated through energy dissipation mechanisms near the tip region rather than being spent on global viscoelastic effects that are known to reduce the strength of solid wood. It also appears that the energy dissipation takes place in such a way that the failure is governed by a maximum energy criterion that is independent of ROL.

The relative magnitude of the average peak load for the four volumes, from the largest to smallest, was in the following proportions: 15: 7.5: 2.38: 1. These values may be compared to the volume, area, and dimension ratios in Table 1 and ascertained that the peak load does not directly reflect these ratios.

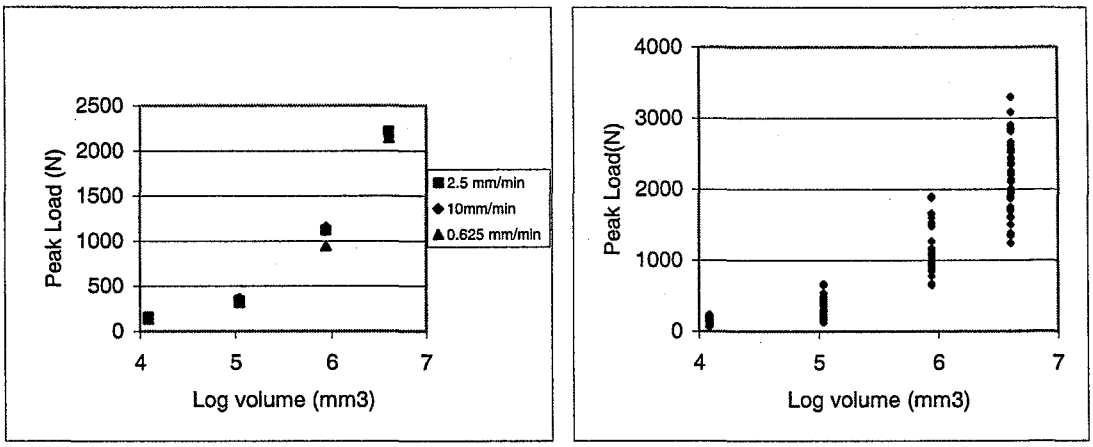

(a) (b)

Fig. 8 Peak load in relation to volume and rate of loading: (a) mean values, and (b) raw data

In wood testing, it is normal to observe a large spread in the data as in Figure 8(b) and in most cases the mean value is used. We hypothesized that the scatter in the peak load in Figure 8(b) could be due to the variation in the physical and geometric data for each specimen. To test this hypothesis, we developed a neural network model to predict the peak load for each beam and study peak load behavior from these variables, namely, LogVolume, LogROL, density, moisture content, Young's modulus, grain angle, face angle, and curvature of growth rings. As pointed out earlier, Young's modulus seemed lower than expected; however, this should not have affected the trends revealed by the neural network because all input variables were normalized between –1 and 1 to achieve a fairer representation of the variables. Since crack length to depth ratio was maintained constant at 0.45, crack length was not included as a variable. Neural networks develop a multi-dimensional function for the dependent variable and in the process, all areas of the domain of the data are traversed to produce the optimum model.

The Neural Network model was developed in a modelling environment called NeuroShell2 (1997) and a Ward net ™, which is a variation of the Multi-Layer Perceptron (MLP) network, was used to model the data. This neural network has one

input layer, two sets of neurons in the hidden layer with each set having a different activation function, and one output layer. The total data set was randomly divided into three sets- 60% for training, 20% for testing the progress in training and stopping before over-fitting starts, and another 20% for validation of the developed network. Only the first two data sets are used in training and the validation set shows the prediction and generalizing ability of the developed network when exposed to new data that it has not seen before.

Figure 9 shows the peak load predicted from the neural network and the actual load for the validation data set. It shows remarkable prediction accuracy with an R^2 value of 0.953 indicating that the neural network has captured 95.3% of the variation of the peak load. The network performed a sensitivity analysis for each variable while holding the others at their mean value and revealed the following order of significance and contribution of the variables to the sensitivity analysis: Log Volume (28%), Young's modulus (18%), curvature (12%), density (9.7%), grain angle (9.5%), moisture content (9.5%), Log ROL (7.3%), and face angle (5.2%).

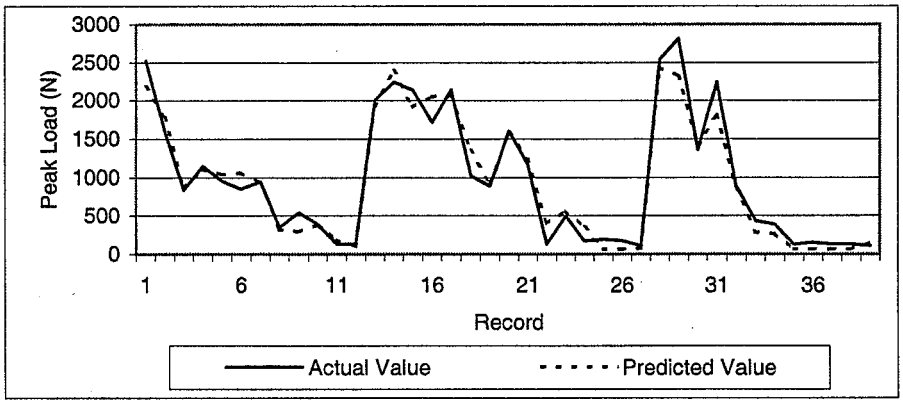

Fig. 9. Actual and neural network predicted peak load

In order to show the combined effect of the variables on the predicted peak load, two variables at a time are plotted in Figures 10 (a), (b), (c), (d), (e), and (f) while other variables being fixed at their mean value. Figure 10(a) shows the combined effect of volume and ROL on peak load and it reveals a markedly nonlinear effect of volume and a negligible effect of ROL, as was also indicated by the mean value plots. There is a slight increase in the peak load for the largest volume at the highest ROL and whether this indicates a trend for larger volumes is not clear. Figure 10(b) shows the combined influence of Young's modulus and volume. The peak load

increases with modulus; however, larger volumes are much more sensitive to modulus than smaller ones.

Figure 10(c) shows the combined effect of moisture content and dry density. Here, lower density and higher moisture content combination results in a higher peak load and vice versa. This contradicts the well-known density and moisture content effects on solid wood and fracture strength (Paterson and Bodig, 1982). However, these are the conditions that increase crack tip plasticity. Porter (1964) demonstrated and explained that moisture acts as a plasticiser at the tip there by increasing strain energy release rate required for fracture. Smith and Chui (1993) observed that the strain energy release rate increased with moisture content up to about 18%. In our study, only one species and kiln-dried specimens from one log were used and therefore, the range of spread of data is not as large as in the studies reported in the literature. However, the moisture and density effects on crack tip behavior needs further investigation.

Figure 10(d) shows the effect of face (ring) angle and grain angle on the peak load, which demonstrates that smaller face angles and smaller grain angles (i.e. grain parallel to the axis of the beam) produce larger peak loads. Figure 10(e) highlights the combined effect of curvature and face angle and it indicates that smaller curvature (i.e. flatter growth rings) and smaller face angles have a greater effect on peak load.

Figure 10(f) shows the combined effect of grain angle and curvature on the peak load. It shows that the peak load is higher for smaller grain angle and curvature. This is realistic because a larger load can be expected for grain parallel to the longitudinal axis of a beam and for flatter growth rings. The results indicate that neural networks are an effective method for predicting load carrying capacity of a cracked beam under the uncertain influence of physical and geometric variables.

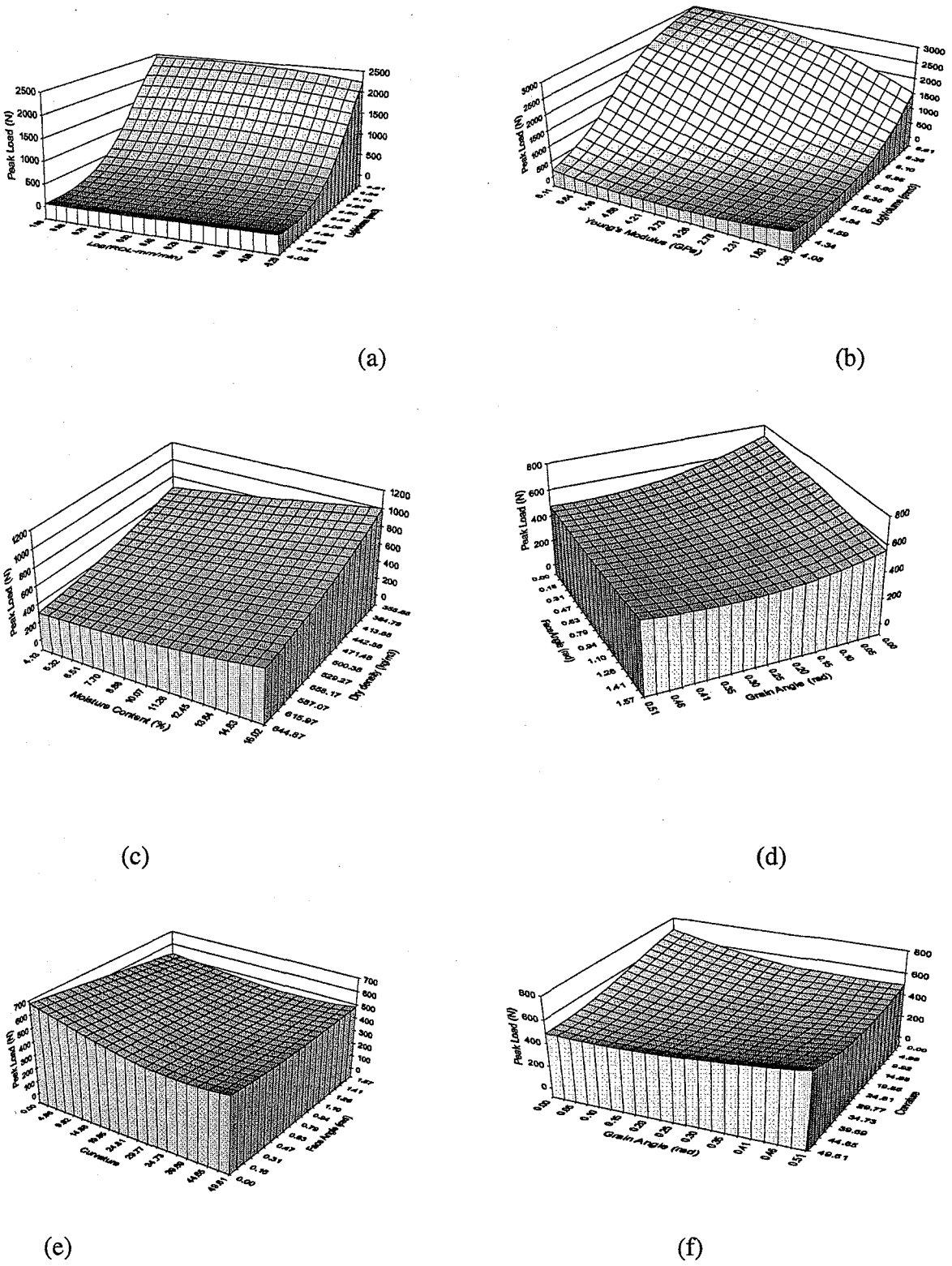

Fig. 10. Combined effect of variables on peak load modeled by the neural network: (a) Log Volume and Log ROL, (b) Young's modulus and Log Volume, (c) moisture content and density, (d) grain angles and face (ring) angle, (e) curvature and face angle, and (f) grain angle and curvature

6.4.2 Crack Initiation Load

Crack initiation load is the load at which the load-deflection graphs deviated from the linear path. A notable observation was that this load was very inconsistent compared to the peak load. Figure 11 shows the average initiation load against volume for the three ROLs that indicates that the volume effect is very pronounced whereas ROL is not. The average crack initiation load follows a power function.

A neural network was developed to predict the crack initiation load for a particular cracked beam with its known physical and geometric data. Figure 12 shows the actual and predicted values for the validation data set. Here, the prediction accuracy was lower than that for the peak load and R^2 value was 0.77. The order of the variables and their contribution to the sensitivity analysis from the most to least significant were: Log Volume (30%), Young's Modulus (14.8%), grain angle (11.2%), curvature (9.9%), face Angle (9.17%), moisture content (9.12%), density (8.22%), and Log ROL (7.65%). Some variables have reversed the order of significance from the peak load analysis but Young's modulus, curvature and grain angle appear to be important secondary variable for both peak and crack initiation loads. The results highlight the usefulness of neural networks for predicting load carrying capacity of a cracked beam at crack initiation. The relative magnitude of the average crack initiation load for the four volumes, from the largest to the smallest, had the following proportions: 10: 5.22: 1.82: 1. These also do not reflect volume, area, or dimension ratios in Table 1.

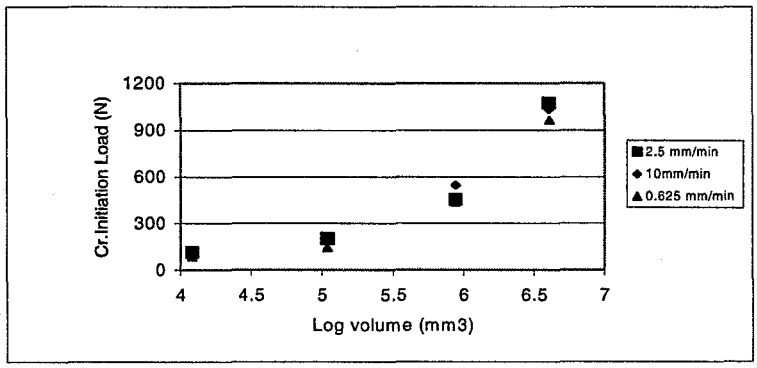

Fig. 11. Average crack initiation load for the three rates of loading

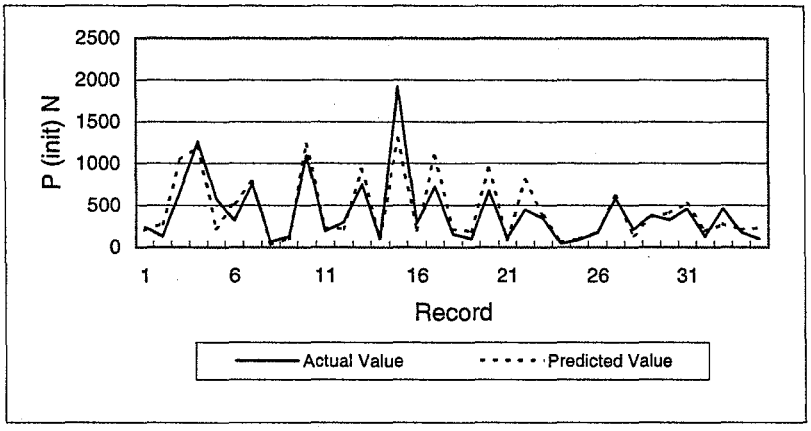

Fig. 12. Actual and neural network predicted crack initiation load

6.5 Peak stress and crack initiation stress

Stress is a material property; however, it has been shown that smaller volumes are stronger than larger volumes due to the lower probability of existence of weakest links in a smaller volume (Griffith, 1920, Madsen, 1992). It has been shown true for solid wood members (Madsen, 1992). In this study, we tested this phenomenon for cracked beams. The plots of average gross stress against volume for the three ROLs showed a marked volume effect on peak stress and no ROL effect. Here, the smallest volume was the strongest. Figure 13 shows the plot of average Log (peak stress) against log (volume) for all speeds, which indeed reveals a linear relationship confirming Weibull's weakest link theory. The Log average gross stress at crack initiation as well as catastrophic failure is also plotted here and they also show a linear relationship with log volume. The net stresses also showed a similar trend. The relative proportion of average peak stress for the four volumes, from the largest to the smallest, was: 1: 1.33: 1.78: 3.33 and initial stress proportions were: 1: 1.19: 2.14: 5.

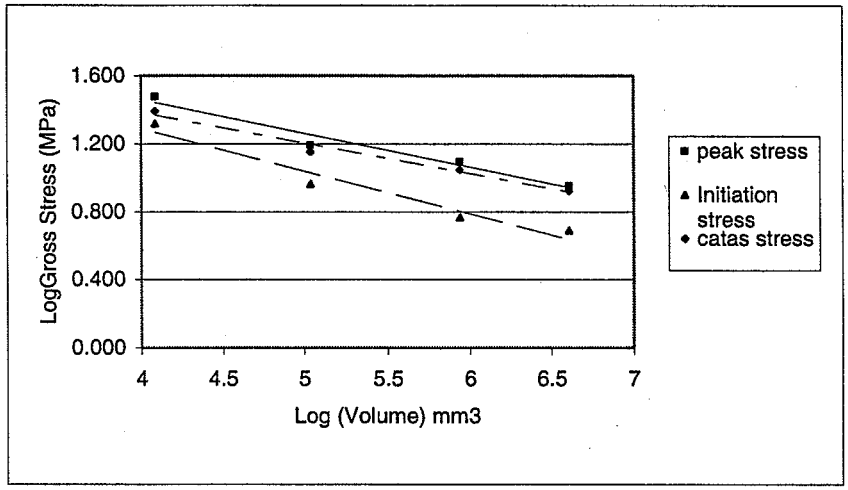

Fig. 13. Log Average gross stresses in relation to LogVolume

Separate neural networks were developed to predict gross peak and initiation stresses for each beam from its physical and geometric variables and the predicted and actual values are shown in Figures 14 and 15.

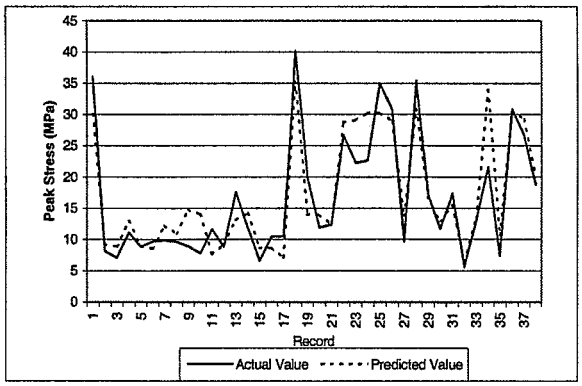

Fig. 14. Actual and neural network predicted peak stress

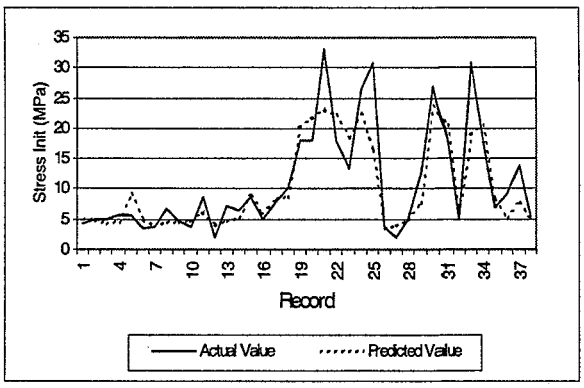

Fig. 15. Actual and neural network predicted crack initiation stress

Peak stress was predicted with R^2 value of 0.87 and initiation stress with an R^2 value of 0.76. Prediction accuracy for peak stress here is slightly lower than that for the peak load with R^2 of 0.953. Various volume, area (e.g. net, gross and other combinations) and dimension ratios that could help explain the size effect on stress were also tested in a variety of neural networks but they did not improve upon the predictions based on volume given in Figure 14 and 15.

6.6 Fracture toughness at crack initiation

An obvious feature and concern in this study was the inconsistency of the crack initiation load, which resulted in the ratio of peak load to crack initiation load ranging from 1 to 5.6. For metals, ASTM standards recommended ratio is 1.1 for a mostly linear load-displacement plot up to failure. In wood beams, there is a large nonlinear region before failure and therefore, the ratio adopted for metals is not suitable. Boontanjay (1979), who tested notched pinus radiata beams, also found a large ratio and he arbitrarily selected 2.5 as being the maximum acceptable ratio for a valid fracture toughness test. Previous investigators have also addressed the need to define a limit for this large ratio (in Boontanjay, 1979). In our study, a ratio of 2.5 was selected and this reduced the data set to 72% of the original set. It is worth noting that the large ratios were more a characteristic of larger volumes. For example, the rejection rate from the largest to smallest volumes was: 31%, 38%, 18%, and 4%.
For the reduced set, the fracture toughness (K_{Ic}) was obtained from the standard formula shown in Eq.(9) (Pilkey, 1994) and associated formulae (Eq.(10) and (11)):

$$K_{Ic} = \sigma\sqrt{\pi a}\ F\left(\frac{a}{h}\right) \qquad [9]$$

$$F\left(\frac{a}{h}\right) = 1.106 - 1.552\left(\frac{a}{h}\right) + 7.71\left(\frac{a}{h}\right)^2 - 13.53\left(\frac{a}{h}\right)^3 + 14.23\left(\frac{a}{h}\right)^4 \qquad [10]$$

$$\sigma = \frac{6P_{init}L}{4bh^2} \qquad [11]$$

where, a is crack length, h is height and b is width of the specimen, L is span, P_{init} is load at crack initiation and σ is the remotely applied stress. Figure 16 shows the relationship between mean fracture toughness and volume for the three ROLs and it indicates that the average fracture toughness follows a power function. The figure shows that the fracture toughness is the largest for the smallest volume and its sensitivity diminishes for larger volumes. The high K_{Ic} for the smallest volume may be depicting plane stress fracture toughness whereas the more constant values represent plane strain fracture toughness. Figure 16 also shows the insignificant role played by the ROL. The log (K_{Ic}) vs. log(Vol) plot was not linear indicating that Weibull type description does not hold.

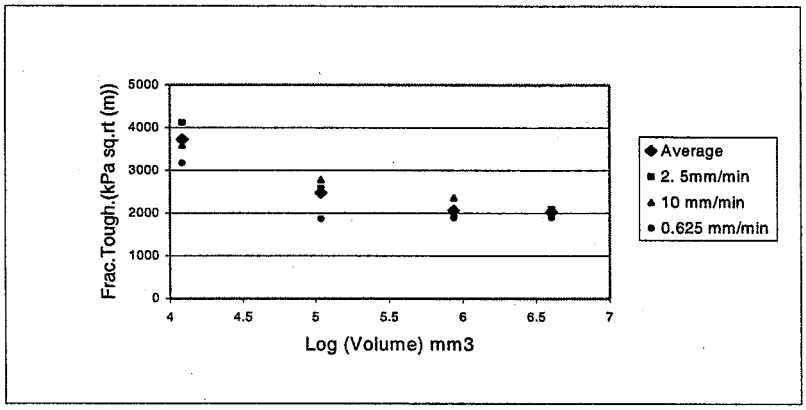

Fig. 16 Volume and ROL effects on mean Fracture toughness

A neural network model developed to predict K_{Ic} for each beam from its properties resulted in an R^2 value of 0.55 and the actual and predicted fracture toughness is shown in Figure 17. In this network, length, width and height, instead of volume that had less predictive power, were used along with other physical and geometric variales. Although the prediction accuracy was not as high as that for loads and stresses, the network produced realistic trends for the combined effect of the physical and geometric variables as was the case for loads and stresses. An especially useful finding from the neural network was that the width had a marked effect on fracture toughness than the length or depth further confirming the plane stress conditions for thinner specimens. Figure 18 shows this in relation to width and height. The order of significance from the sensitivity analysis was: width, height, Young's modulus, face angle, length, grain angle, ROL, moisture content, and density.

As noted earlier, peak load for all the volumes was more consistent and predictable than the crack intiation load. Therefore, fractrue toughness based on peak load may be a more reliable indicator of strength. However, there is a large nonlinear region which requires an appropriate method for determining the fracture toughness. Assuming that the crack growth is insiginificant upto the peak load, a pseudo fracture toughness at peak load was also calculated from Eq (9) and was found to be much less sensitive to the smaller volumes than the K_{Ic} based on the initiaiton load. Furthermore, the relative magnitude of the normalizing or the geometric coefficient of the K_{Ic} formula in Eq(9) (i.e. $6 L\sqrt{\pi a}/(4 b d^2)$) for the four volumes, from largest to smallest, were: 1: 2.17: 6.26: 17. These values follow peak load ratios (15: 7.5: 2.38: 1) more closely than they do intiation load ratios (10: 5.22: 1.82: 1).

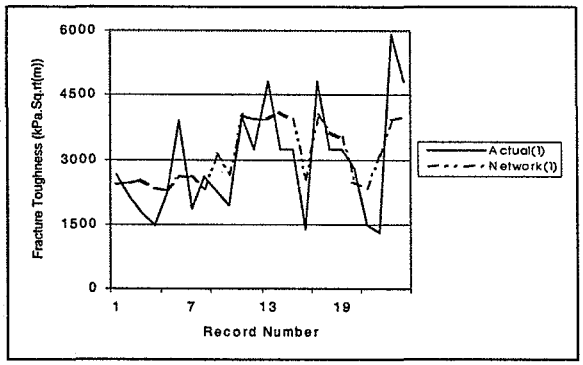

Fig. 16. Actual and ANN predicted fracture toughness

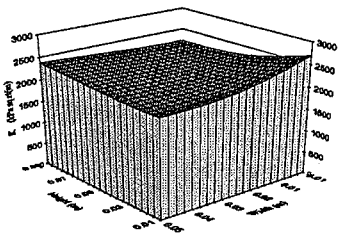

Fig. 17 Width and height effect on fracture toughness as predicted by the neural network model

The reduced data set was used to redo the crack intiation load and correspoding stress investigation discussed in sections 6.4 and 6.5. The exclusion of the specimens with high peak to initiation load ratios had only a very slight effect on the mean values and their trends of larger volumes, and no effect on neural network predictions.

7. Summary and Conclusions

This study has been an exploration of fracture properties and systematically and step-by-step dealt with the major issues concerning the behavior of cracked wood beams. The volume effect on DOL to initiation was more marked at the smallest ROL and it was almost inhibited at the largest ROL. Furthermore, the largest volume was much more negatively influenced by ROL indicating that larger volumes could hold the load disproportionately longer up to initiation at lower ROLs. The DOL for propagation was a random phenomenon for a particular size category. However, the largest volume failed more quickly at the lowest ROL indicating that for yet smaller ROLs, catastrophic failure could be more imminent for larger volumes after crack initiaiton. This phenomenon needs further study. The crack propagation was a wave phenomenon leading to negative and positive speeds, especially at higher ROLs, reaching the highest at the catastrophic failure.

Both the peak and crack initiation loads were insensitive to ROL and negatively correlated with volume. However, the peak load was very consistent whereas crack initiation load was not. Average of both loads follow power functions. The most successful ANN model was developed to predict the peak load for each

beam from physical and geometric variables including volume, ROL, Young's modulus, density, moisture content, grain angle, curvature of growth rings and face angle. Plots of the combined effect of variables on the peak load showed realistic trends; however, the effect of moisture content and density was contrary to the accepted trends and needs further investigation. Due to the inconsistency of the initiation load, ANN prediction accuracy for it was lower. The results indicated that volume was the predominant variable and Young's modulus, grain angle, and curvature were the most important secondary variables affecting peak and initiaiton loads.

The average gross crack intiation and peak stresses were insensitive to ROL and nonlinearly related to volume with the smallest volume exhibiting the largest stress. The volume effect on initiation, peak, and catastrophic stresses agreed with Weibull's weakest link theory. Neural network models were also developed to predict the peak and initiation stresses of individual beams with high accucracy but the prediction accuracy for peak stress was slightly less than that for the peak load.

Fracture toughness for initiation was insensitive to ROL. It was the largest for the smallest volume and the mean fracture toughness followed a power function. The neural network model developed to predict toughness of each beam showed that the width has a much greater influence on fracture toughness than length and height confirming the plane stress conditions that lead to larger fracture toughness values for thinner specimens. The ANN prediction accuracy for fracture toughness was not as high as that for loads and stresses. The order of the three most important variables were: width, height, and Young's modulus. A more comprehensive study is needed to check the applicability of the results to a wider domain. The exclusion of specimens with high peak to initiation load ratios had little or no effect on the results. Fracture toughness based on peak load may be a more reliable indicator of strength if appropriate methods are used to incorporate nonlinearity.

The insensitivity of load carrying capacity of cracked beams to ROL is contrary to the well-known viscoelastic effects on wood and needs further investigation.

The study showed that the neural networks were a very useful tool for predicting load carrying capacity of individual beams from their properties and for analysing their trends. The current study was of exploratory nature and dealt with only a limited range of values for the variables. However, it is promising that, with

further refinements and a larger database representing a larger range of values, ANNs have the potential to be reliable predictors of load capacity of cracked bodies under the uncertain influence of physical and geometric variables. These could be maximum load, stress or fracture toughness.

References:

1. Abraham, F.E., (1997) Portrait of a crack; Rapid Fracture Mechanics using parallel molecular dynamics. J. IEEE. Comp. Sci. and Eng., IBM Almaden Research Centre, pp.66-77.
2. ASTM Standards- Metal testing, (1995) E 1290- section 1290- page 869.
3. ASTM Standards-Wood, 1995, D 143.
4. Barrett, D. and Foschi, R.O., (1978) On the application of brittle fracture theory, fracture mechanics and creep-rupture models for the prediction of the reliability of wood structural elements, Proc.First Int.Conf. on Wood Frac., pp.1-37.
5. Boontanjay, C. (1979) Fracture toughness of New Zealand pinus radiata. ME Thesis. Univ. of Auckland, New Zealand.
6. Dharmasiri Bandara, D.M., Samarasinghe, S. and Mackenzie, D.W. (1999) High-speed video imaging to study effect of volume and speed of testing on fracture dynamics of wood. Proc. Pacific Timber Eng. Conf. pp. 300-307.
7. Griffith, A.A. (1920) The phenomena of rupture and flow in solids. Phil. Trans. Roy. Soc. Of London, Vol.A221, 163.
8. Haykin, S. (1994). Neural Networks: A comprehensive Foundation, MacMillan College Pub. Co., New York.
9. Johnson, J.A. (1973) Crack initiation in wood plates. Wood Sci. 6(2):151-158
10. Madsen, B., (1992) Structural behaviour of timber, pp:128, 129, 153, 177, 241.
11. Mindness, S., Madison, B., and Barrett, J.D., (1978) Rate of loading and duration of load tests on Douglas-fir in tension perpendicular to the grain. Proc. First Int. Conf.on Wood Frac., pp. 143-157.
12. Nielsen, L.F., (1978) Crack failure of dead-, ramp-, and combined-loaded viscoelastic materials, Proc. First Int. Conf. on Wood Frac., pp.187-200.
13. Patton-Mallory, M., & Cramer, S. (1987) Fracture mechanics: a tool for predicting wood component strength. For. Prod. J. 37(7/8):39-47.

14. Pederson, M.U., Clorius, C.O., Damkidle, P., Hoffmeyer, P. and Traberg, S. (1999) Size effect in tension perpendicular to the grain. Dept. of Struc.Eng. and Materials, Tech. Univ.of Denmark, DK 2800 Lyngby, pp207-214.

15. Petterson, R.W. and Bodig, J. (1982) Prediction of fracture toughness of conifers. Wood and Fib.Sci. 15(4):302-316.

16. Porter, A.W. (1964). On the mechanics of fracture in wood. For.Prod.J. Vol.14:325-331

17. Samarasinghe, S and Kulasiri, G.D. (2000(a)) Displacement Fields of wood in tension based on image processing: Part 1. Tension parallel- and perpendicular-to-grain and comparisons with isotropic behavior, Silva Fennica 34(3): 251-259.

18. Samarasinghe, S and Kulasiri, G.D. (2000(b)) Displacement Fields of wood in tension based on image processing: Part 2. Crack-tip displacements in Mode-I and Mixed Mode fracture. Silva Fennica 34(3): 260-273.

19. Samarasinghe, S and Kulasiri, G.D. (1999) Fracture toughness of wood based on experimental near-tip displacements and orthotropic fracture theory, Proc. Pacific Timber Eng. Conf. pp. 292-299.

20. Samarasinghe, S and Kulasiri, G.D. (1998) Investigation of stress intensity factors of wood using image processing and orthotropic fracture theory. Proceeding of the 12th Eng.Mech.Conf. pp.618-621.

21. Schniewind, A.P., Bartels, H.J. and Gammon, B.W. (1978) Effect of pre-loading on fracture toughness of wood. Proc.1st Int. Conf. on Wood Frac. pp. 227-238.

22. Sih, G.C., Paris, P.C. and Irwin, G.R. (1965). On cracks in rectilinearly anisotropic bodies. Int. J.Frac.Mech. 1:189-203.

23. Smith, I. And Chui, Y.H. (1993). Factors affecting mode I fracture energy of plantation-grown red pine. Wood Sci. and Tech. pp.

24. Smith, M. (1996) Neural networks for statistical modelling. Int. Thomson Comp. Press.

25. Spencer, R.A., (1978) Rate of loading effect of bending for Douglas-fir, Proc. 1st Int.Conf.on Wood Fract., Forinteck Canada Corp., Vancouver, Canada, pp.259-280

26. Stanzl-Tschegg, S.E., Tan, D.M. and Tschegg, E.K. (1995) New splitting method for wood fracture characterization. Wood Sci.and Tech. pp.31-50.